The Parabolic Variance (PVAR): A Wavelet Variance Based on the Least-Square Fit

François Vernotte, Michel Lenczner, Pierre-Yves Bourgeois, and Enrico Rubiola

Abstract—This paper introduces the parabolic variance (PVAR), a wavelet variance similar to the Allan variance (AVAR), based on the linear regression (LR) of phase data. The companion article arXiv:1506.05009 [physics.ins-det] details the Ω frequency counter, which implements the LR estimate. The PVAR combines the advantages of AVAR and modified AVAR (MVAR). PVAR is good for long-term analysis because the wavelet spans over 2τ, the same as the AVAR wavelet, and good for short-term analysis because the response to white and flicker PM is $1/\tau^3$ and $1/\tau^2$, the same as the MVAR. After setting the theoretical framework, we study the degrees of freedom and the confidence interval for the most common noise types. Then, we focus on the detection of a weak noise process at the transition—or *corner*—where a faster process rolls off. This new perspective raises the question of which variance detects the weak process with the shortest data record. Our simulations show that PVAR is a fortunate tradeoff. PVAR is superior to MVAR in all cases, exhibits the best ability to divide between fast noise phenomena (up to flicker FM), and is almost as good as AVAR for the detection of random walk and drift.

Index Terms—Allan variance, atomic frequency standard, flicker, frequency noise, frequency stability, measurement uncertainty, oscillator, phase noise.

I. INTRODUCTION

THE ALLAN variance (AVAR) was the first of the wavelet-like variances used for the characterization of oscillators and frequency standards [1]. After 50 years of research, AVAR is still unsurpassed at rendering the largest τ for a given time series of experimental data. This feature is highly desired for monitoring the frequency standards used for timekeeping.

Unfortunately, AVAR is not a good choice in the region of fast noise processes. In fact, the AVAR response to white and flicker PM noise is nearly the same, $1/\tau^2$. For short-term analysis, other wavelet variances are preferred, chiefly the modified AVAR (MVAR) [2]–[4]. The MVAR response is $1/\tau^3$ and $1/\tau^2$ for white and flicker PM, respectively. However, MVAR is poor for slow phenomena because the wavelet spans over 3τ instead of 2τ. Thus, for a data record of duration T, the absolute maximum τ is $T/3$ instead of $T/2$.

F. Vernotte is with the UTINAM, Observatory THETA, University of Franche-Comté/UBFC/CNRS, 25010 Besançon, France (e-mail: francois.vernotte@obs-besancon.fr).

M. Lenczner, P.-Y. Bourgeois, and E. Rubiola are with the CNRS, Department of Time and Frequency (UBFC, UFC, UTBM, ENSMM), FEMTO-ST Institute, 25000 Besançon, France (e-mail: michel.lenczner@femto-st.fr; pyb2@femto-st.fr; rubiola@femto-st.fr).

Speaking of "wavelet-like" variances, we review the fundamentals. A wavelet $\psi(t)$ is a shock with energy equal to one and average equal to zero, whose energy is well confined in a time interval (see, e.g., [5, p. 2]) called "support" in proper mathematical terms. In formula, $\int_{\mathbb{R}} \psi^2(t)\,dt = 1$, $\int_{\mathbb{R}} \psi(t)\,dt = 0$, and $\int_{-a/2}^{a/2} \psi^2(t)\,dt = 1 - \epsilon$, with small $\epsilon > 0$. It makes sense to renormalize the wavelet as $\frac{1}{a}\int_{\mathbb{R}} \psi^2(t)\,dt = 1$, so that it is suitable to power-type signals (finite power) instead of energy-type signals (energy finite). By obvious analogy, we use the terms "power-type wavelet" and "energy-type wavelet." These two normalizations often go together in spectral analysis and telecom (see the classical books [6] and [7]). For historical reasons, in clock analysis, we add a trivial coefficient that sets the response to a linear drift D_y to $\frac{1}{2}D_y^2$, the same for all the variances.

High resolution in the presence of white and flicker phase noise is mandatory for the measurement of short-term fluctuations (μs to s), and useful for medium-term fluctuations (up to days). This is the case of optics and the generation of pure microwaves from optics. The same features are of paramount importance for radars, VLBI, geodesy, space communications, etc. As a fringe benefit, extending the time-domain measurements to lower τ is useful to check on the consistency between variances and phase noise spectra. MVAR is suitable to the analysis of fast fluctuations, at a moderate cost in terms of computing power. Frequency counters specialized for MVAR are available as a niche product, chiefly intended for research labs [8].

A sampling rate of $1/\tau$ is sufficient for the measurement of AVAR, while a rate of $1/\tau_0 = m/\tau$ is needed for MVAR, where the rejection of white phase noise is proportional to m. MVAR is based on the simple averaging of m fully overlapped (spaced by the sampling step τ_0) frequency data, before evaluating $\sigma^2(\tau)$.

The linear regression (LR) provides the lowest-energy (or lowest-power) fit of a data set, which is considered in most cases as the optimal approximation, at least for white noise. For our purposes, the least-square fit finds an obvious application in the estimation of frequency from a time series of phase data, and opens the way to improvements in fluctuation analysis. Besides, new digital hardware—like field-programmable gate arrays (FPGAs) and systems on chip (SoCs)—provides bandwidth and computing power at an acceptable complexity, and makes possible least-square fitting in real time.

We apply least-square estimation of frequency to fast time stamping. The simplest estimator in this family is the LR on phase data. The LR can be interpreted as a weight function applied to the measured frequency fluctuations. The shape of

such weight function is parabolic. The corresponding instrument is called "Ω counter," described in the companion article [9]. The name Ω comes from the graphical analogy of the parabola with the Greek letter, in the continuity of the Π and Λ counters [10], [11]. The Ω estimator is similar to the Λ estimator, but exhibits higher rejection of the instrument noise, chiefly of white phase noise. This is important in the measurement of fast phenomena, where the cutoff frequency f_H is necessarily high, and the white phase noise is integrated over the wide analog bandwidth that follows.

In the same way as the Π and Λ estimators yield the AVAR and the MVAR, respectively, we define a variance based on the Ω estimator. Like in the AVAR and MVAR, the weight functions are similar to wavelets, but for the trivial difference that they are normalized for power-type signals. A similar use of the LR was proposed independently by Benkler *et al.* [12] at the IFCS, where we gave our first presentation on the Ω counter and on our standpoint about the PVAR. In a private discussion, we agreed on the name parabolic variance (PVAR) for this variance, superseding earlier terms [13].

We stress that the wavelet variances are mathematical tools to describe the frequency stability of an oscillator (or the fluctuation of any physical quantity). Albeit they have similar properties, none of them should be taken as "the stability" of an oscillator. For the same reason, MVAR and PVAR should not be mistaken as "estimators" of the AVAR. To this extent, the only privilege of AVAR is the emphasis it is given in standard documents [14].

After setting the theoretical framework of the PVAR, we provide the response to noise described by the usual polynomial spectrum. Then, we calculate the degrees of freedom and confidence intervals, checking on the analytical results against extensive simulations. Finally, we compare the performance of AVAR, MVAR, and PVAR for the detection of noise types, using the value of τ where $\sigma^2(\tau)$ changes law as an indicator. In most practical cases, PVAR turns out to be the fastest, to the extent that it enables such detection with the shortest data record.

II. STATEMENT OF THE PROBLEM

The clock signal is usually written as

$$v(t) = V_0 \sin[2\pi\nu_0 t + \varphi(t)]$$

where V_0 is the amplitude, ν_0 is the nominal frequency, and $\varphi(t)$ is the random phase fluctuation. Notice that $\varphi(t)$ is allowed to exceed $\pm\pi$. Alternatively, randomness is ascribed to the frequency fluctuation $(\Delta\nu)(t) = 2\pi\dot{\varphi}(t)$.

We introduce the normalized quantities

$$\mathbf{x}(t) = t + \mathrm{x}(t)$$
$$\mathbf{y}(t) = 1 + \mathrm{y}(t)$$

where $\mathrm{x}(t) = \varphi(t)/2\pi\nu_0$ and $\mathrm{y}(t) = \dot{\mathrm{x}}(t)$. The quantity $\mathbf{x}(t)$ is the clock readout, which is equal to the time t plus the random fluctuation $\mathrm{x}(t)$. Accordingly, the clock signal reads

$$v(t) = V_0 \sin[2\pi\nu_0 \mathbf{x}(t)]$$
$$= V_0 \sin[2\pi\nu_0 t + 2\pi\nu_0 \mathrm{x}(t)].$$
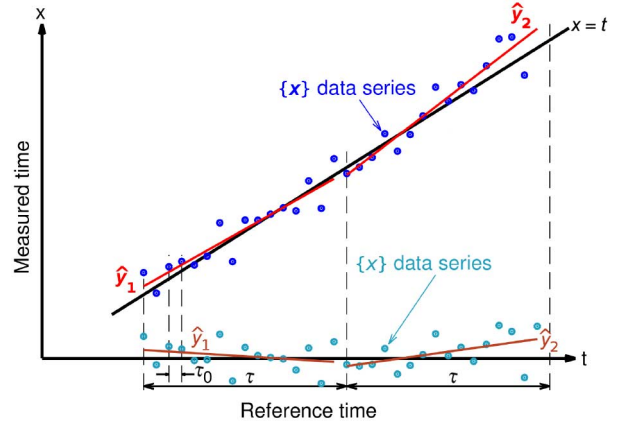
Fig. 1. Principle of two-sample LR measurement and notation.

For the layman, $\mathbf{x}$ is the time displayed by a watch, t is the "exact" time from a radio broadcast, and x the watch error. The error x is positive (negative) when the watch leads (lags). Similarly, $\mathbf{y}$ is the normalized frequency of the watch's internal quartz, and y its fractional error. For example, if y = +10ppm (constant), the watch leads uniformly by 1.15 s/day. For the scientist, $\mathrm{x}(t)$ is the random time fluctuation, often referred to as "phase time" (fluctuation), and $\mathrm{y}(t)$ is the random fractional-frequency fluctuation. The quantities $\mathrm{x}(t)$ and $\mathrm{y}(t)$ match exactly $x(t)$ and $y(t)$ used in the general literature of time and frequency, respectively [14]–[16].

The main point of this paper is explained in Fig. 1. We use the LR of phase data to get a sequence $\{\hat{\mathbf{y}}\}$ of data averaged on contiguous time intervals of duration τ, and in turn the sequence $\{\hat{\mathrm{y}}\}$ of fractional-frequency fluctuation data. Two contiguous elements of $\{\hat{\mathbf{y}}\}$ and $\{\hat{\mathrm{y}}\}$ are shown in Fig. 1, from which we get one value of $\frac{1}{2}(\mathrm{y}_2 - \mathrm{y}_1)^2$ for the estimation of the variance.

Most of the concepts below are expressed in both the continuous and the discrete settings with common notations without risk of confusion. For example, the same expression $\mathbf{x} = t + \mathrm{x}$ maps into $\mathbf{x}_k = t_k + \mathrm{x}_k$ in the discrete case, and into $\mathbf{x}(t) = t + \mathrm{x}(t)$ in the continuous case. The notations $\langle . \rangle$, $(\cdot, \cdot)$, and $||.||$ represent the average, the scalar product, and the norm. They are defined as $\langle \mathbf{x} \rangle = \frac{1}{n}\sum_k \mathbf{x}_k$, $(\mathbf{x}, \mathbf{y}) = \frac{1}{n}\sum_k \mathbf{x}_k\mathbf{y}_k$, $||\mathbf{x}|| = (\mathbf{x}, \mathbf{x})^{1/2}$ where n is the number of terms of the sum in the discrete case, and as $\langle \mathbf{x} \rangle = \frac{1}{T}\int \mathbf{x}(t)\, dt$, $(\mathbf{x}, \mathbf{y}) = \frac{1}{T}\int \mathbf{x}(t)\mathbf{y}(t)\, dt$, $||\mathbf{x}|| = (\mathbf{x}, \mathbf{x})^{1/2}$ where T is the length of the interval of integration in the continuous case. The span of the sum and the integral will be made precise in each case of application. The mathematical expectation and the variance of random variables are denoted by $\mathbb{E}\{\cdot\}$ and $\mathbb{V}\{\cdot\}$.

The LR problem consists in searching the optimum value $\hat{\mathbf{y}}$ of the slope η (dummy variable) that minimizes the norm of the error $\mathbf{x} - \mathbf{x}_0 - \eta t$, i.e., $\hat{\mathbf{y}} = \arg\min_\eta ||\mathbf{x} - \mathbf{x}_0 - \eta t||^2$. Since we are not interested in $\mathbf{x}_0$, which only reflects choice of the origin of $\mathbf{x}$, the solution is the random variable

$$\hat{\mathbf{y}} = \frac{(\mathbf{x} - \langle \mathbf{x} \rangle, t - \langle t \rangle)}{||t - \langle t \rangle||^2}.$$

We recall some useful properties of $\hat{\mathbf{y}}$ as an estimator of the slope of $\mathbf{x}$. For the sake of simplicity, with no loss of generality,

we refer to a time sequence which is centered at zero, i.e., $\langle t \rangle = 0$.

1) The estimator $\hat{\mathbf{y}}$ can be simplified as

$$\hat{\mathbf{y}} = \frac{(\mathbf{x}, t)}{||t||^2}.$$

2) If the component $\mathbf{x}_k$ (or the values $\mathbf{x}(t)$) is independent, the estimator variance is

$$\mathbb{V}\{\hat{\mathbf{y}}\} = \frac{\sigma_\mathbf{x}^2}{||t||^2}.$$

The assumption of independent continuous random process is rather usual in theoretical works. However, this is done to simplify some proofs, the results can be used in their discrete form.

3) Sampling uniformly at the interval τ_0, the discrete time is $t_k = (k + \frac{1}{2})\tau_0$ for $k \in \{-p, \dots, p\}$, $m = 2p$, and $\tau = m\tau_0$. For large m, we get

$$\hat{\mathbf{y}} \approx 1 + \frac{12\,(\mathbf{x}, t)}{m\tau^2} \qquad \text{and} \qquad \mathbb{V}\{\hat{\mathbf{y}}\} \approx \frac{12\sigma_\mathbf{x}^2}{m\tau^2}.$$

4) With a signal that is continuous over a symmetric time interval $(-\frac{\tau}{2}, \frac{\tau}{2})$, we get

$$\hat{\mathbf{y}} = 1 + \frac{12\,(\mathbf{x}, t)}{\tau^3}. \tag{1}$$

The continuous form of the estimator $\hat{\mathbf{y}}$ can be expressed as a weighted average of $\mathbf{x}$ or $\mathbf{y}$. For this purpose, it is useful to take $\hat{\mathbf{y}}$ as a time-dependent function defined over $t \in (0, \tau)$

$$\begin{aligned}
\hat{\mathbf{y}}(t) &= \frac{12}{\tau^3} \int_{-\tau/2}^{\tau/2} s\, \mathbf{x}(t - \tau/2 + s)\, ds \\
&= \frac{12}{\tau^3} \int_{-\tau}^{0} (s + \tau/2)\, \mathbf{x}(t + s)\, ds \\
&= \frac{12}{\tau^3} \int_{0}^{\tau} (\tau/2 - s)\, \mathbf{x}(t - s)\, ds.
\end{aligned} \tag{2}$$

III. Time-Domain Representation

A. Generic Wavelet Variance

Let us denote with T the duration of the data run, with τ_0 the sampling interval, with N the number of samples, and with n the ratio T/τ. Thus, $T = N\tau_0$ and $N = mn$. We consider the series $\{\hat{\mathbf{y}}_i\}_{i=1,\dots,n}$ of frequency deviation estimates. In this section, we denote with $\sigma^2(\tau)$ a generic wavelet variance, either AVAR, MVAR, PVAR, etc.

In the case of uncorrelated frequency fluctuations (white FM), an unbiased estimator of the variance $\mathbb{V}\{\hat{\mathbf{y}}\}$ is

$$S_{n-1}^2 = \frac{1}{n-1} \sum_{i=1}^{n} \left(\hat{\mathbf{y}}_i - \frac{1}{n} \sum_{j=1}^{n} \hat{\mathbf{y}}_j \right)^2$$

so

$$\mathbb{V}\{\hat{\mathbf{y}}\} = \mathbb{E}\{S_{n-1}^2\}.$$

After Allan [1], we replace the estimator S_{n-1}^2 with a two-sample variance by setting $n = 2$. Then, the variance $\mathbb{V}\{\hat{\mathbf{y}}\} = \mathbb{E}\{S_1^2\}$ is

$$\sigma^2(\tau) = \frac{1}{2}\mathbb{E}\left\{ (\hat{\mathbf{y}}_1 - \hat{\mathbf{y}}_2)^2 \right\} \tag{3}$$

and its estimator averaged over the $n - 1$ terms

$$\hat{\sigma}^2(\tau) = \frac{1}{2} \left\langle \left(\hat{\mathbf{y}}_i - \hat{\mathbf{y}}_{i+1} \right)^2 \right\rangle. \tag{4}$$

Notice that two-sample variance is generally written as $\sigma_\mathbf{y}^2(\tau)$, and that we drop the subscript y.

Following the Lesage–Audoin approach [17], we define the point variance estimates

$$\alpha_i = \frac{1}{\sqrt{2}} \left(\hat{\mathbf{y}}_i - \hat{\mathbf{y}}_{i+1} \right) \tag{5}$$

and the estimated variance

$$\hat{\sigma}^2(\tau) = \frac{1}{M} \sum_{i=1}^{M} \alpha_i^2. \tag{6}$$

The relationship between the α_i and the N individual $\mathbf{x}(k\tau_0)$ measures depends on the type of counter (Π, Λ, Ω).

B. Continuous-Time Formulation of PVAR

In the case of continuous time, the difference between contiguous measures is

$$\begin{aligned}
\hat{\mathbf{y}}(t + \tau) - \hat{\mathbf{y}}(t) &= \frac{12}{\tau^3} \left[\int_0^\tau \left(\frac{\tau}{2} - s \right) \mathbf{x}(t + \tau - s)\, ds \right. \\
&\qquad \left. - \int_0^\tau \left(\frac{\tau}{2} - s \right) \mathbf{x}(t - s)\, ds \right] \\
&= \frac{12}{\tau^3} \int_{-\tau}^\tau \left(|s| - \frac{\tau}{2} \right) \mathbf{x}(t - s)\, ds \\
&= \frac{12}{\tau^3} \int_{-\tau}^\tau \left(|t - s| - \frac{\tau}{2} \right) \mathbf{x}(s)\, ds.
\end{aligned}$$

Accordingly, the two-sample variance (3) is written as

$$\sigma_P^2(\tau) = \frac{1}{2}\mathbb{E}\left\{ (\hat{\mathbf{y}}(t + \tau) - \hat{\mathbf{y}}(t))^2 \right\}$$

and notice the subscript P for PVAR. Such variance is independent of t, and it can be expressed as the running average

$$\sigma_P^2(\tau) = \mathbb{E}\left\{ \left(\int_{-\tau}^{+\tau} \mathbf{x}(s)\, w_\mathbf{x}(s - t)\, ds \right)^2 \right\} \tag{7}$$

where

$$w_\mathbf{x}(t) = \frac{6\sqrt{2}}{\tau^3} \left(|t| - \frac{\tau}{2} \right) \chi_{(-\tau, \tau)}(t)$$

is the even weight function, and

$$\chi_{(-\tau, \tau)}(t) = \begin{cases} 1, & t \in (-\tau, \tau) \\ 0, & \text{elsewhere} \end{cases}$$

is the indicator function (or characteristic function).

From (7), we see that PVAR can also be written as a convolution product

$$\sigma_P^2(\tau) = \mathbb{E}\left\{\left(\int_{-\infty}^{+\infty} \mathrm{x}(s)\,\hbar_\mathrm{x}(t-s)\,ds\right)^2\right\}$$

$$= \mathbb{E}\left\{(\mathrm{x}(t) * \hbar_\mathrm{x}(t))^2\right\}$$

where $\hbar(t)$ is the convolution kernel which applies to $\mathrm{x}(t)$. The kernel $\hbar(t)$ is related to the weight function $w(t)$ by the general property that $\hbar(t) = w(-t)$. However, since $w_\mathrm{x}(t)$ is even function, it holds that $\hbar_\mathrm{x}(t) = w_\mathrm{x}(t)$.

Similarly, the estimator (4) is written as

$$\sigma_P^2(\tau) = \mathbb{E}\left\{\frac{1}{T}\int_0^T [\mathrm{y}(t) * \hbar_\mathrm{y}(t)]^2 \; dt\right\} \tag{8}$$

where

$$\hbar_\mathrm{y}(t) = \frac{3\sqrt{2}\,t}{\tau^3}\,(|t| - \tau)\,\chi_{(-\tau,\tau)}(t) \tag{9}$$

is the convolution kernel which applies to $\mathrm{y}(t)$.

Thanks to the fact that $\mathrm{y}(t) = \dot{\mathrm{x}}(t)$, $\sigma_P^2(\tau)$ can also be expressed as the running average

$$\sigma_P^2(\tau) = \mathbb{E}\left\{\left(\int_{\mathbb{R}} \mathrm{y}(s)\,w_\mathrm{y}(s-t)\,ds\right)^2\right\}$$

where

$$w_\mathrm{y}(t) = -\frac{3\sqrt{2}\,t}{\tau^3}\,(|t| - \tau)\,\chi_{(-\tau,\tau)}(t)$$

is the weight function. Since $w_\mathrm{y}(t)$ is odd function, it holds that $\hbar_\mathrm{y}(t) = -w_\mathrm{y}(t)$. Moreover, the parabolic shape of the PVAR wavelet comes from the $t \cdot |t|$ factor in $w_\mathrm{y}(t)$ and $\hbar_\mathrm{y}(t)$.

For the purpose of operation with the Fourier transform, it is convenient to restate these expression in terms of filter or convolution

$$\sigma_P^2(\tau) = \mathbb{E}\{(\mathrm{y} * \hbar_\mathrm{y})^2\} = \mathbb{E}\{(\mathrm{x} * \hbar_\mathrm{x})^2\}. \tag{10}$$

The weight functions $w_\mathrm{x}(t)$ and $w_\mathrm{y}(t)$, and also the kernels $\hbar_\mathrm{x}(t)$ and $\hbar_\mathrm{y}(t)$, match the definition of power-type wavelet given in Section I. As a consequence of the property $\mathrm{y}(t) = \dot{\mathrm{x}}(t)$, it holds that $\hbar_\mathrm{x}(t) = \dot{\hbar}_\mathrm{y}(t)$. Fig. 2 shows the convolution kernels associated to PVAR.

It is worth pointing out that our formulation is in general, as it applies to AVAR, MVAR, PVAR, and other similar variances as well. Of course, the wavelet depends on the counter (Fig. 3).

C. Practical Evaluation of PVAR

Denoting the discrete time with $\mathrm{x}_i = \mathrm{x}(i\tau_0)$, the estimate of the two-sample variance is [17]

$$\alpha_i = \frac{1}{\sqrt{2}\,\tau}\,(-\mathrm{x}_i + 2\mathrm{x}_{i+m} - \mathrm{x}_{i+2m}) \tag{11}$$

for AVAR, with $M = N - 2m$, and

$$\alpha_i = \frac{1}{\sqrt{2}\,m\tau}\sum_{k=0}^{m-1}(-\mathrm{x}_{i+k} + 2\mathrm{x}_{i+m+k} - \mathrm{x}_{i+2m+k}) \tag{12}$$
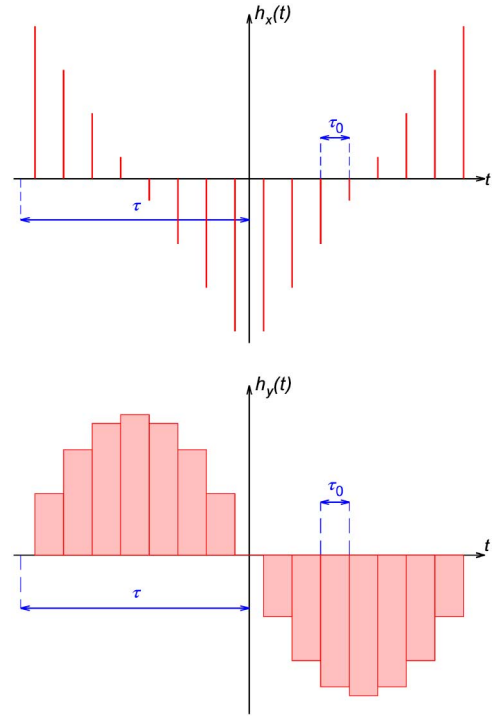
Fig. 2. Convolution kernels of PVAR from phase data (above) or frequency deviations (below) for $\tau = 8\tau_0$.
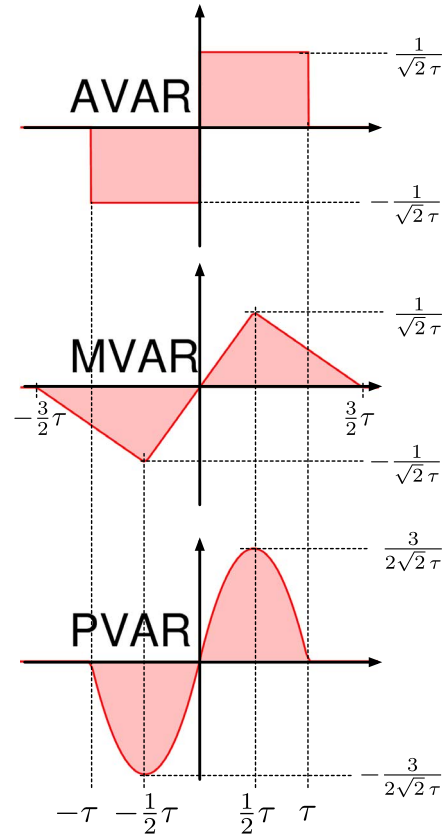
Fig. 3. Wavelets associated to AVAR, MVAR, and PVAR.

for MVAR, with $M = N - 3m + 1$.

Now, we calculate α_i for PVAR. First, the discrete form of $\hat{y}$ can be obtained from (2) by replacing the time integral with

a sum with a time increment equal to τ_0. Accordingly, τ is replaced with $m\tau_0$, s with $k\tau_0$, t with $i\tau_0$, and $x(t)$ with x_i

$$\hat{y}_i = \frac{12}{m^3\tau_0^3} \sum_{k=0}^{m-1} \left(\frac{(m-1)\tau_0}{2} - k\tau_0 \right) x_{i-k}\tau_0$$

$$= \frac{12}{m^2\tau} \sum_{k=0}^{m-1} \left(\frac{m-1}{2} - k \right) x_{i-k}.$$

Similarly,

$$\hat{y}_{i+1} = \frac{12}{m^2\tau} \sum_{k=0}^{m-1} \left(\frac{m-1}{2} - k \right) x_{i+m-k}$$

and consequently

$$\hat{y}_i - \hat{y}_{i+1} = \frac{12}{m^2\tau} \sum_{k=0}^{m-1} \left(\frac{m-1}{2} - k \right) (x_{i-k} - x_{i+m-k}).$$

Second, we recall that x_i is defined for $i \geq 0$. Hence, we have to shift the origin by $m - 1$, so that also $\hat{y}_i$ is defined with $i = 0$

$$\hat{y}_i - \hat{y}_{i+1} = \frac{12}{m^2\tau} \sum_{k=0}^{m-1} \left(\frac{m-1}{2} - k \right)$$
$$\times (x_{i+m-1-k} - x_{i+2m-1-k}).$$

Third, since the coefficient $(m-1)/2 - k$ is symmetrical for k and $m - 1 - k$, we interchange $i + m - 1 - k$ with $i + m - 1 - (m - 1 - k) = i + k$, and $i + 2m - 1 - k$ with $i + 2m - 1 - (m - 1 - k) = i + m + k$

$$\hat{y}_i - \hat{y}_{i+1} = \frac{12}{m^2\tau} \sum_{k=0}^{m-1} \left(\frac{m-1}{2} - k \right) (x_{i+k} - x_{i+m+k}).$$

Finally, it comes

$$\alpha_i = \frac{6\sqrt{2}}{m^2\tau} \sum_{k=0}^{m-1} \left(\frac{m-1}{2} - k \right) (x_{i+k} - x_{i+m+k})$$
$$\text{for } m \geq 2 \qquad (13)$$
$$M = N - 2m + 2.$$

For consistency with AVAR and MVAR, we require $\sigma_P^2(\tau_0) = \sigma_A^2(\tau_0) = \sigma_M^2(\tau_0)$, i.e., all variances are equal at sampling time τ_0. Since (13) gives $\alpha_i = 0$ for $m = 1$, we redefine

$$\alpha_i = \frac{1}{\sqrt{2}\tau_0} (-x_i + 2x_{i+1} - x_{i+2}), \qquad \text{for } m = 1 \quad (14)$$
$$M = N - 2.$$

Having N samples $\{x_i\}$ taken at the interval τ, the estimate $\hat{\sigma}_P^2(\tau)$ can be computed using (6) and (13) as

$$\hat{\sigma}_P^2(\tau) = \frac{72}{Mm^4\tau^2} \sum_{i=0}^{M-1} \left[\sum_{k=0}^{m-1} \left(\frac{m-1}{2} - k \right) (x_{i+k} - x_{i+m+k}) \right]^2.$$
$$(15)$$
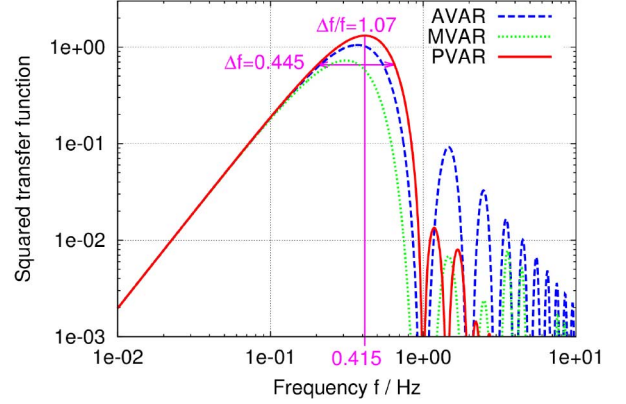
Fig. 4. PVAR transfer function, compared to AVAR and MVAR, for integration time is $\tau = 1$ s and sampling interval $\tau_0 = \tau/4 = 250$ ms.

D. Time-Domain Response

From (15), it comes

$$\sigma_P^2(\tau) = \mathbb{E}\left\{ \hat{\sigma}_P^2(\tau) \right\}$$

$$= \frac{72}{m^4\tau^2} \mathbb{E}\left\{ \frac{1}{M} \sum_{i=0}^{M-1} \left[\sum_{k=0}^{m-1} \left(\frac{m-1}{2} - k \right) (x_{i+k} - x_{i+m+k}) \right] \right.$$
$$\left. \times \left[\sum_{l=0}^{m-1} \left(\frac{m-1}{2} - l \right) (x_{i+l} - x_{i+m+l}) \right] \right\}$$

$$= \frac{72}{m^4\tau^2} \sum_{k=0}^{m-1} \sum_{l=0}^{m-1} \left(\frac{m-1}{2} - k \right) \left(\frac{m-1}{2} - l \right)$$
$$\times [R_x((k-l)\tau_0) - R_x((k-m-l)\tau_0)$$
$$- R_x((m+k-l)\tau_0) + R_x((k-l)\tau_0)] \qquad (16)$$

where $R_x(\theta) = \mathbb{E}\{x(t)x(t+\theta)\}$ is the autocorrelation function of $x(t)$. The autocorrelation function is detailed in Section V-D, whereas $R_x(\tau)$ depends on f_L and f_H, these parameters cancel in the derivation of PVAR.

IV. FREQUENCY DOMAIN REPRESENTATION

A. Transfer Function

The transfer function $H_P(f)$ of PVAR is the Fourier transform of the kernel $\mathfrak{h}_y(t)$. The square of its modulus is given by

$$|H_P(f)|^2 = \frac{9 \left[2\sin^2(\pi\tau f) - \pi\tau f \sin(2\pi\tau f) \right]^2}{2(\pi\tau f)^6}. \qquad (17)$$

Fig. 4 shows $|H_P(f)|^2$, together with the transfer function of AVAR and MVAR. All are bandpass functions with approximately one octave bandwidth. However, PVAR exhibits significantly smaller sidelobes because the weight function is smoother. This is well known with the taper (window) functions used in the digital Fourier transform [18].

This can be proved as follows. The transfer function is obtained after Fourier transformation, using the property that $\mathfrak{h}_y$ is odd function

TABLE I
RESPONSE OF AVAR, MVAR, AND PVAR TO THE COMMON NOISE TYPES AND DRIFT

Noise type	$S_y(f)$	AVAR $\sigma_A^2(\tau)$	MVAR $\sigma_M^2(\tau)$	PVAR $\sigma_P^2(\tau)$	$\dfrac{\sigma_P^2(\tau)}{\sigma_M^2(\tau)}$
White PM	$h_2 f^2$	$\dfrac{3h_2}{8\pi^2\tau_0\tau^2}$	$\dfrac{3h_2}{8\pi^2\tau^3}$	$\dfrac{3h_2}{2\pi^2\tau^3}$	4
Flicker PM	$h_1 f^1$	$\dfrac{[1.038 + 3\ln(\pi\tau/\tau_0)]\,h_1}{4\pi^2\tau^2}$	$\dfrac{[24\ln(2) - 9\ln(3)]\,h_1}{8\pi^2\tau^2}$	$\dfrac{3\,[\ln(16) - 1]\,h_1}{2\pi^2\tau^2}$	3.2
White FM	$h_0 f^0$	$\dfrac{h_0}{2\tau}$	$\dfrac{h_0}{4\tau}$	$\dfrac{3h_0}{5\tau}$	2.4
Flicker FM	$h_{-1} f^{-1}$	$2\ln(2)h_{-1}$	$\dfrac{[27\ln(3) - 32\ln(2)]\,h_{-1}}{8}$	$\dfrac{2\,[7 - \ln(16)]\,h_{-1}}{5}$	1.8
Random walk FM	$h_{-2} f^{-2}$	$\dfrac{2\pi^2 h_{-2}\tau}{3}$	$\dfrac{11\pi^2 h_{-2}\tau}{20}$	$\dfrac{26\pi^2 h_{-2}\tau}{35}$	1.4
Drift	$y(t) = D_y t$	$\dfrac{1}{2}D_y^2\tau^2$	$\dfrac{1}{2}D_y^2\tau^2$	$\dfrac{1}{2}D_y^2\tau^2$	1

The lowpass cutoff frequency f_H, needed for AVAR, is set to $1/2\tau_0$ (Nyquist frequency).

$$H_y(f) = \int_{\mathbb{R}} \mathfrak{h}_y(t) e^{-2i\pi f t} dt$$
$$= \frac{12i}{\sqrt{2\tau^3}} \Im\left\{\int_0^\tau t\,(t - \tau)\,e^{-2i\pi f t}\,dt\right\}.$$

The primitive is calculated by parts integration

$$\int_0^\tau t\,(t - \tau)\,e^{-2i\pi f t} dt = \frac{1}{4\pi^3 f^3}\left(\pi\tau f - ie^{-2i\pi\tau f}\right.$$
$$\left. +\pi\tau f e^{-2i\pi\tau f} + i\right).$$

Then,

$$H_P(f) = \frac{3i}{\sqrt{2}\pi^3\tau^3 f^3}\left[1 - \cos(2\pi\tau f) - \pi\tau f \sin(2\pi\tau f)\right].$$

Finally, using $1 - \cos(2\pi\tau f) = 2\sin^2(\pi\tau f)$, we get

$$H_P(f) = \frac{3i}{\sqrt{2}\pi^3\tau^3 f^3}\left[2\sin^2(\pi\tau f) - \pi\tau f \sin(2\pi\tau f)\right]$$

and

$$|H_P(f)|^2 = \frac{9}{2\pi^6\tau^6 f^6}\left[1 - \cos(2\pi\tau f) - \pi\tau f \sin(2\pi\tau f)\right]^2.$$

B. Convergence Properties

For small f, it holds that

$$\sin(\pi\tau f) \approx \pi\tau f - \frac{1}{6}\pi^3\tau^3 f^3 + O(f^5)$$
$$\sin(2\pi\tau f) \approx 2\pi\tau f - \frac{4}{3}\pi^3\tau^3 f^3 + O(f^5)$$

so

$$2\sin^2(\pi\tau f) - \pi\tau f \sin(2\pi\tau f) \approx 2\left(\pi\tau f - \frac{1}{6}\pi^3\tau^3 f^3\right)^2$$
$$- \pi\tau f\left(2\pi\tau f - \frac{4}{3}\pi^3\tau^3 f^3\right) + f^5 O(f)$$
$$\approx \frac{1}{18}\pi^4\tau^4 f^4\left(\pi^2\tau^2 f^2 + 12\right) + f^5 O(f)$$

then, at low frequency,

$$H_P(f) \approx \sqrt{2} i\pi\tau f.$$

We conclude that

$$|H_P(f)|^2 \approx 2\pi^2\tau^2 f^2 \quad \text{at low frequency}$$

thus PVAR converges for $1/f^2$ FM noise. Similarly,

$$|H_P(f)|^2 \propto (\pi\tau f)^{-4} \quad \text{at high frequency}$$

therefore, PVAR converges for f^2 FM noise.

C. Calculation of PVAR From Spectral Data

Given the power spectral density (PSD) $S_x(f)$, PVAR evaluated as

$$\sigma_P^2(\tau) = \int_0^\infty |H_P(f)|^2 S_y(f)\,df. \qquad (18)$$

Replacing $S_y(f)$ with the components of the polynomial law, from $h_{-2}f^{-2}$ (random walk FM) to $h_2 f^2$ (white PM), we get the response shown in Table I, together with AVAR and MVAR.
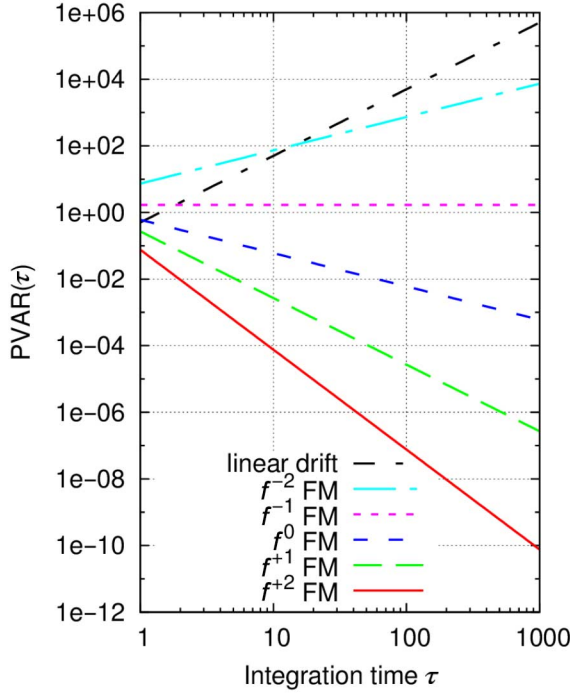
Fig. 5. Response of PVAR to the polynomial-law noise types and linear drift.

Fig. 5 shows the response of PVAR to the polynomial-law noise types as a function of the integration time τ.

For comparison, $\sigma_P^2(\tau)$ can also be calculated in the time domain using (16), and also with Monte Carlo simulations (see Section V-E). Time domain, frequency domain, and Monte Carlo simulations give fully consistent results.

V. DEGREES OF FREEDOM AND CONFIDENCE INTERVAL

A. Equivalent Degrees of Freedom (EDF)

We consider the estimates of a generic variance $\sigma^2(\tau)$, assumed $k\chi_\nu^2$-distributed, $k \in \mathbb{R}^+$. The EDF ν depend on the integration time τ, and of course on the noise type. The mean and variance (the variance of the variance) are

$$\begin{aligned} \mathbb{E}\left\{\hat{\sigma}^2(\tau)\right\} &= k\mathbb{E}\left\{\chi_\nu^2\right\} = k\nu \\ \mathbb{V}\left\{\hat{\sigma}^2(\tau)\right\} &= k^2\mathbb{V}\left\{\chi_\nu^2\right\} = 2k^2\nu. \end{aligned}$$

Accordingly, the degrees of freedom ν are given by

$$\nu = \frac{2\,\mathbb{E}\left\{\hat{\sigma}^2(\tau)\right\}^2}{\mathbb{V}\left\{\hat{\sigma}^2(\tau)\right\}}. \tag{19}$$

Thus, the knowledge of ν enables to define a confidence interval around $\mathbb{E}\left\{\hat{\sigma}^2(\tau)\right\}$ with given confidence p. For applying this result to PVAR, we have then to calculate the variance of PVAR.

B. Variance of PVAR

The variance of the estimate $\hat{\sigma}^2(\tau)$ is given by

$$\begin{aligned} \mathbb{V}\left\{\hat{\sigma}^2(\tau)\right\} &= \mathbb{E}\left\{\left[\hat{\sigma}^2(\tau) - \mathbb{E}\left\{\hat{\sigma}^2(\tau)\right\}\right]^2\right\} \\ &= \mathbb{E}\left\{\left[\frac{1}{M}\sum_{i=0}^{M-1}\alpha_i^2 - \mathbb{E}\left\{\frac{1}{M}\sum_{i=0}^{M-1}\alpha_i^2\right\}\right]^2\right\}. \end{aligned} \tag{20}$$

Expanding (20) yields

$$\mathbb{V}\left\{\hat{\sigma}^2(\tau)\right\} = \frac{1}{M^2}\sum_{i=0}^{M-1}\sum_{j=0}^{M-1}\left[\mathbb{E}\left\{\alpha_i^2\alpha_j^2\right\} - \mathbb{E}\left\{\alpha_i^2\right\}\mathbb{E}\left\{\alpha_j^2\right\}\right].$$

Isserlis's theorem [19]–[21] states that, for centered and jointly Gaussian random variables z and w

$$\mathbb{E}\left\{z^2w^2\right\} - \mathbb{E}\left\{z^2\right\} - \mathbb{E}\left\{w^2\right\} = 2\left[\mathbb{E}\left\{zw\right\}\right]^2.$$

Assuming that x is a Gaussian process and that α_i, α_j are two centered jointly Gaussian random variables, it comes

$$\mathbb{V}\left\{\hat{\sigma}^2(\tau)\right\} = \frac{2}{M^2}\sum_{i=0}^{M-1}\sum_{j=0}^{M-1}\left[\mathbb{E}\left\{\alpha_i\alpha_j\right\}\right]^2. \tag{21}$$

The derivation of $\mathbb{E}\left\{\alpha_i\alpha_j\right\}$ is given in Section V-C.

C. EDF of PVAR

From (13), we can calculate

$$\mathbb{E}\left\{\alpha_i\alpha_j\right\} = \frac{72}{m^4\tau^2}\mathbb{E}\left\{\left[\sum_{k=0}^{m-1}\left(\frac{m-1}{2}-k\right)(x_{i+k}-x_{i+m+k})\right]\right.$$
$$\left.\times\left[\sum_{l=0}^{m-1}\left(\frac{m-1}{2}-l\right)(x_{j+l}-x_{j+m+l})\right]\right\}$$

which expands as

$$\begin{aligned} \mathbb{E}\left\{\alpha_i\alpha_j\right\} = \frac{72}{m^4\tau^2}\sum_{k=0}^{m-1}\sum_{l=0}^{m-1}&\left(\frac{m-1}{2}-k\right)\left(\frac{m-1}{2}-l\right) \\ &\{2R_x[(i+k-j-l)\tau_0] \\ &- R_x[(i+k-j-m-l)\tau_0] \\ &- R_x[(i+m+k-j-l)\tau_0]\}. \end{aligned} \tag{22}$$

Thanks to (21) and (22), we can calculate the variance of PVAR from the autocorrelation function $R_x(\tau)$. For example, in the case of white PM noise we find

$$\mathbb{V}\left\{\hat{\sigma}_P^2(\tau)\right\} = \frac{9\mathbf{h}_2^2}{70\pi^4\tau^6}\left[23\frac{m}{M} - 12\left(\frac{m}{M}\right)^2 - 175\frac{m}{M^2}\right] \tag{23}$$

and

$$\nu = \frac{35}{23m/M - 12(m/M)^2 - 175m/M^2}. \tag{24}$$

D. Numerical Evaluation of the EDF

The EDF can be evaluated by substituting (22) into (21), and then (21) into (19). In turn, thanks to the Wiener Khinchin theorem, stationary ergodic processes state that $R_x(\tau)$ can be obtained as the inverse Fourier transform of the PSD. Since the PSD is real and even [22], [23], we get

$$R_x(\tau) = \int_0^{+\infty} S_x(f)\cos(2\pi\tau f)\,df. \tag{25}$$

TABLE II
AUTOCORRELATION FUNCTION OF THE PHASE-TIME FLUCTUATION

$S_x(f)$	$R_x(0)$	$R_x(\tau)$ (for $\tau \neq 0$)
k_0	$k_0 f_H$	0
$k_{-1}f^{-1}$	$k_{-1}\left[\dfrac{1}{2}+\ln(f_H/f_L)\right]$	$k_{-1}\left[\dfrac{\cos(2\pi f_L\tau)-1+2\pi f_L\tau\sin(2\pi f_L\tau)}{(2\pi f_L\tau)^2}+\text{Ci}(2\pi\tau f_H)-\text{Ci}(2\pi\tau f_L)\right]$
$k_{-2}f^{-2}$	$k_{-2}\left[\dfrac{1}{f_L}-\dfrac{1}{f_H}\right]$	$k_{-2}\left\{\dfrac{\cos(2\pi f_L\tau)}{f_L}-\dfrac{\cos(2\pi f_H\tau)}{f_H}+2\pi\tau\left[\text{Si}(2\pi f_L\tau)-\text{Si}(2\pi f_H\tau)\right]\right\}$
$k_{-3}f^{-3}$	$\dfrac{k_{-3}}{2}\left[\dfrac{1}{f_L^2}-\dfrac{1}{f_H^2}\right]$	$k_{-3}\left\{\dfrac{\cos(2\pi f_L\tau)}{2f_L^2}-\dfrac{\cos(2\pi f_H\tau)}{2f_H^2}+2\pi^2\tau^2\left[\text{Ci}(2\pi f_L\tau)-\text{Ci}(2\pi f_H\tau)\right]+\pi\tau\left[\dfrac{\sin(2\pi f_H\tau)}{f_H}-\dfrac{\sin(2\pi f_L\tau)}{f_L}\right]\right\}$
$k_{-4}f^{-4}$	$\dfrac{k_{-4}}{3}\left[\dfrac{1}{f_L^3}-\dfrac{1}{f_H^3}\right]$	$k_{-4}\left\{\dfrac{(2\pi^2 f_H^2\tau^2-1)\cos(2\pi f_H\tau)+\pi f_H\tau\sin(2\pi f_H\tau)}{3f_H^3}-\dfrac{(2\pi^2 f_L^2\tau^2-1)\cos(2\pi f_L\tau)+\pi f_L\tau\sin(2\pi f_L\tau)}{3f_L^3}+\dfrac{4\pi^3\tau^3}{3}\left[\text{Si}(2\pi f_H\tau)-\text{Si}(2\pi f_L\tau)\right]\right\}$

f_L and f_H are the highpass and lowpass cutoff frequencies which set the process bandwidth. Ci(x) and Si(x) are the cosine and sine integral functions.
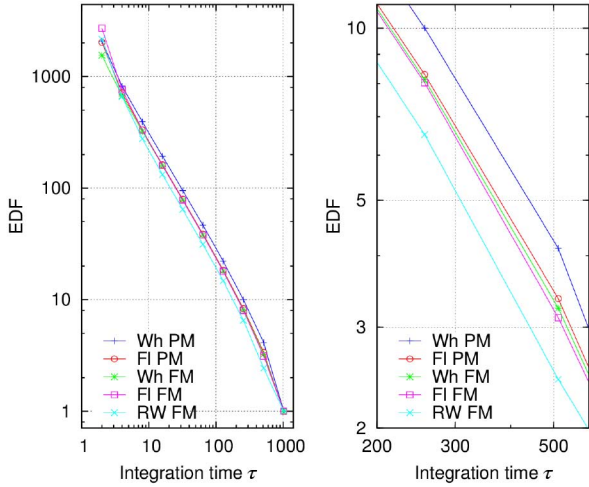
Fig. 6. Numerical computation of the PVAR EDF for the common noise types. The right-hand plot is a crop of the left one.

Fig. 7. Comparison of the EDF calculated analytically (24), by numerical computation (Section V-D), and assessed by Monte Carlo simulation (Section V-E).

Replacing $S_x(f)$ with the polynomial law from white PM to random walk FM (f^{-4} PM), we get the results shown in Table II. The derivation is rather mechanical, and done by a symbolic algebra application (Wolfram Mathematica). For numerical evaluation—unless the reader understanding the computer code in depth—we recommend the approximations $\lim_{\to 0}\text{Ci}(x)=C+\ln(x)-x^2/96$, where $C\approx 0.5772$ is the Euler–Mascheroni constant, $\lim_{x\to\infty}\text{Ci}(x)=0$, $\lim_{x\to 0}\text{Si}(x)=x-x^3/9$, and $\lim_{x\to\infty}\text{Si}(x)=\pi/2$.

As an example, we take a data record of $N=2048$, $\tau_0=1$ s, high cut-off frequency $f_H=\frac{1}{2\tau_0}$ (equal to the Nyquist frequency), low cut-off frequency $f_L=\frac{1}{256 N\tau_0}$

(see [23] for the physical meaning of f_L), and $\tau \in \{\tau_0, 2\tau_0, 4\tau_0, \ldots, 1024\tau_0\}$. Fig. 6 shows the EDF for the common noise types. Zooming in (Fig. 6 right), we see that the plots do not overlap.

E. Monte Carlo Simulations

Another way to assess the EDF is by simulated time series. We generated 10 000 sequences of $N=2048$ samples for each type of noise using the *bruiteur* noise simulator [24], which is based on filtered white noise. This code is a part of the SigmaTheta software package, available on the URL given by [24]. It has been validated by more than 20 years of intensive use at the Observatory of Besancon. Again, the EDF are calculated using (19).

TABLE III
COMPARISON OF THE EDF OF AVAR, MVAR, AND PVAR FOR THE COMMON NOISE TYPES

τ/τ_0	1	2	4	8	16	32	64	128	256	512	682	1024
White PM (f^{+2} FM)												
AVAR	892	1060	1020	1010	955	953	922	896	811	652		0.981
MVAR	891	970	685	355	173	82.5	38.9	17.3	7.48	2.88	1.02	
PVAR	892	1150	824	419	202	99.1	46.9	22.0	10.0	4.13		1.03
Flicker PM (f^{+1} FM)												
AVAR	1090	1140	984	728	523	340	209	127	69.5	33.8		0.930
MVAR	1090	1020	544	258	126	62.1	29.3	13.9	5.73	2.09	1.04	
PVAR	1090	1300	701	329	165	79.4	38.2	18.4	8.42	3.36		1.05
White FM (f^0 FM)												
AVAR	1380	1200	716	372	186	91.7	45.3	21.8	10.2	4.07		1.01
MVAR	1380	1060	505	247	119	58.4	28.6	13.2	5.71	1.87	1.04	
PVAR	1380	1390	680	319	157	76.7	37.5	18.2	8.43	3.32		1.01
Flicker FM (f^{-1} FM)												
AVAR	1780	1200	595	299	150	72.8	36.1	17.1	7.58	3.05		1.02
MVAR	1780	1030	484	241	120	57.9	28.5	12.9	5.32	1.58	1.02	
PVAR	1780	1470	648	319	159	77.8	38.2	18.2	8.01	3.16		1.02
Random walk FM (f^{-2} FM)												
AVAR	1990	1020	480	238	117	57.9	28.1	13.3	5.93	2.29		1.01
MVAR	1990	861	398	197	96.5	47.1	22.6	10.3	4.26	1.31	1.02	
PVAR	1990	1290	548	266	131	64.3	31.2	14.8	6.53	2.49		1.02

In the end, we compared three methods, the autocorrelation function $R_x(\tau)$ with (21) and (22), the Monte Carlo simulation with *bruiteur* code, and the analytical solution (24), the latter only with white noise. Fig. 7 compares the EDF obtained with these three methods. The results match well, with a discrepancy of a few percent affecting only the first two points ($\tau \leq 2\tau_0$). The reason is that, with such a small τ/τ_0 ratio, the w_y weight function is a poor approximation of the parabola of the Ω counter (see [9]).

Table III and Fig. 8 compare the EDF of PVAR to AVAR and MVAR. MVAR is limited to $\tau = 682$ because the wavelet support (span) is 3τ instead of 2τ.

VI. DETECTION OF NOISE PROCESSES

Running an experiment, we accumulate a progressively larger number N of samples x_k. As N gets larger, we fill up the $\hat{\sigma}_y^2(\tau)$ plot adding new points at larger τ. Besides, at smaller τ, the error bars shrink because the number of degrees of freedom increases. Looking at the log–log plot, we find the fast processes on the left and the slow processes on the right. This is due to the nearly polynomial law τ^k of Table I. Having said that, we address the question of which variance is the most efficient tool at detecting a slower process "**SP**" in the presence of a faster process "**FP**" as illustrated in Fig. 9. The criterion we choose is the lowest level of the **SP** that can be detected:

1) with a probability of 97.5% (i.e., two sigma upper bound);
2) in the presence of the faster process **FP** of given level;
3) using a data record of given length N.

Our question about the most efficient tool relates to relevant practical cases detailed underneath.

Our comparison is based on a simulation with $N = 2048$ samples uniformly spaced by $\tau_0 = 1$ s. So, the lowest τ is equal to 1 s, and the largest τ is equal to $N\tau_0/2 = 1024$ s for AVAR and PVAR, and to $N\tau_0/3 = 682$ s for MVAR.

For fair comparison, we renormalize the variances for the same response to the **SP** process. For example, the response

to white FM noise $S_y(f) = \mathbf{h}_0$ is $\mathbf{h}_0/2\tau$ for the AVAR, $\mathbf{h}_0/4\tau$ for the MVAR, and $3\mathbf{h}_0/5\tau$ for the PVAR. Accordingly, a coefficient of 2, 4, or 5/3 is applied, respectively. Of course, this renormalization makes sense only for comparison, and should not be used otherwise.

The results are shown in Fig. 10, and discussed in Sections VI-A to VI-C. Each simulation is averaged on 10^4 runs. All plots show AVAR (blue), MVAR (green), and PVAR (red) for the **FP** process, with the two-sigma uncertainty bars, and the **SP** process (gray). We set the reference value of the **SP** process at the lowest level that PVAR can detect with a probability of 97.5%, i.e., at the upper point of the two-sigma uncertainty bar at $\tau = 1024$ s. This is highlighted by a gray circle at $\tau = 1024$ s.

A. Noise Detection in the Presence of White PM Noise [Fig. 10(a) and (b)]

White PM noise is a limiting factor in the detection of other noise processes because it is the dominant process in the front-end of most instruments used to assess the frequency stability. We show the effect of white PM in two opposite cases, white FM noise and frequency drift. The former is present in all atomic standards, while the latter is present in all oscillators and standards, except in the primary standards. Frequency drift is a severe limitation in cavity stabilized lasers, and in other precision oscillators based on the mechanical properties of an artifact.

The classical AVAR is clearly a poor option because of its τ^{-2} response to white PM, versus the τ^{-3} of the other variances. This is confirmed in our simulations.

It is seen in Fig. 10(a) and (b) that in both cases MVAR cannot detect the slow process. The lowest value of MVAR (green plot) at 97.5% confidence (gray circle at $\tau = 682$ s) exceeds the reference gray line.

The conclusion is that PVAR exhibits the highest detection sensitivity in the presence of white PM noise.
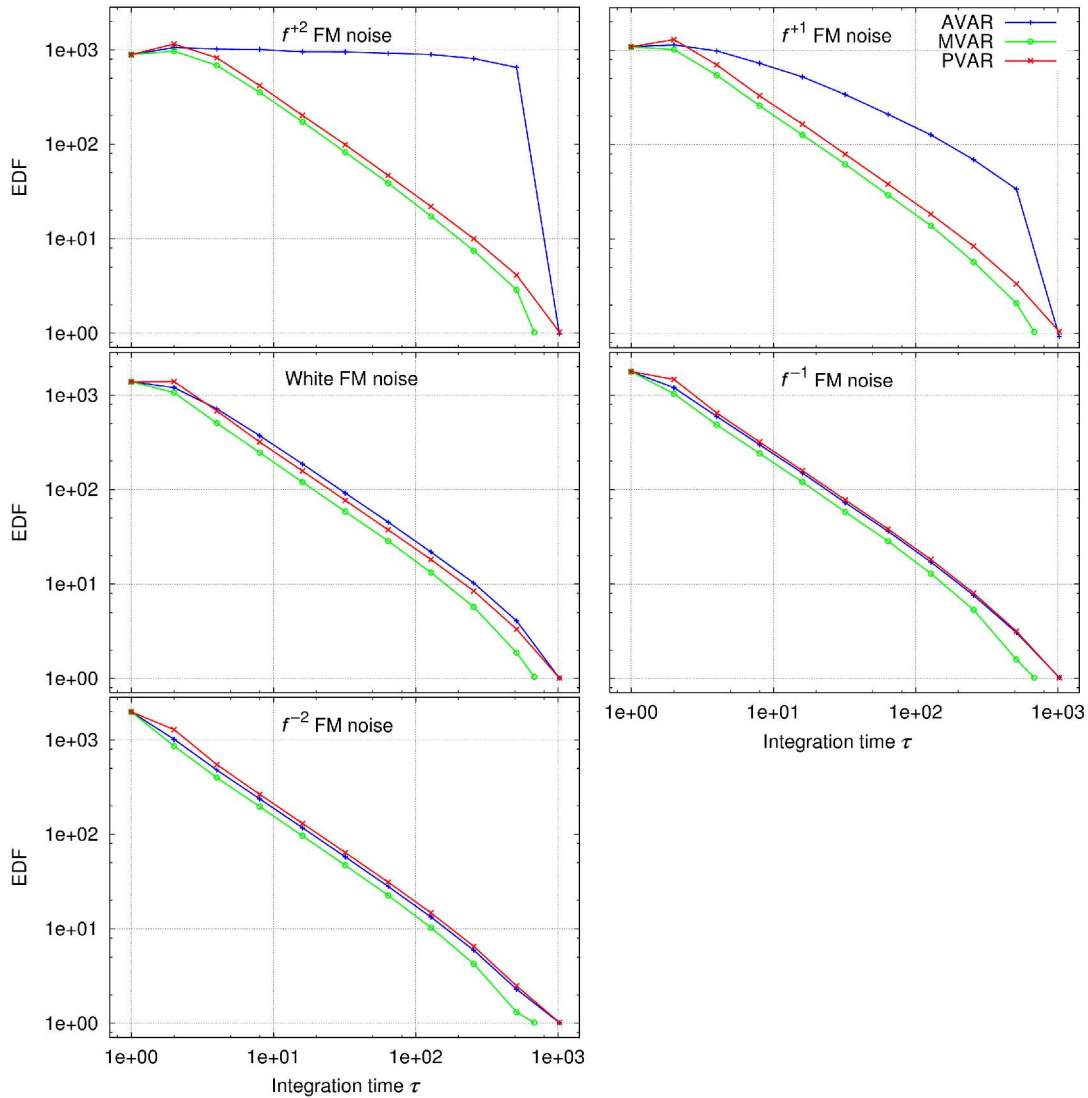
Fig. 8. Comparison of the EDF of AVAR, MVAR, and PVAR for the different types of noise. All noise sequences were simulated with a unity coefficient noise, 2048 samples, and a sampling frequency of 1 Hz.
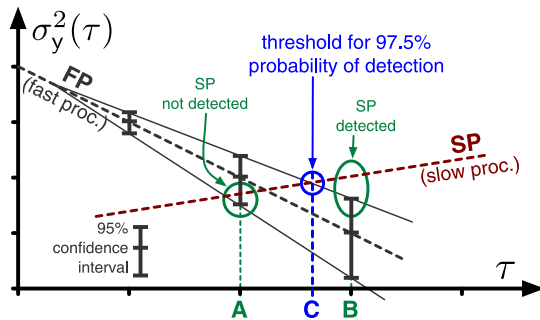
Fig. 9. Concept of noise process detection. The process **SP** is barely visible in A ($<50\%$ probability), detected with a probability of 97.5% in C (threshold of nearly certain detection), and detected with $>97.5\%$ probability in B.

B. Detection of Flicker FM Noise in the Presence of White FM Noise [Fig. 10(c)]

The detection of frequency flicker in the presence of white FM noise is a typical problem of passive atomic standards. Such standards show white FM noise originated from the signal-to-noise ratio, and in turn from beam intensity, optical contrast, or other parameters depending on the physics of the standard. Generally, after the white FM noise rolls off, $\sigma_y^2(\tau)$ hits the flicker floor. Cs clocks are a special case because they do not suffer from random walk and drift. So, flicker of frequency is the ultimate limitation to long-term stability, and in turn to timekeeping accuracy. In commercial standards, flicker FM exceeds the white FM at approximately 1-day integration time. Thus, fast detection of flicker enables early estimation of the long-term behavior, and provides a useful diagnostic.

We see in Fig. 10(c) that the three variances show similar performances, with a small superiority of AVAR and PVAR. Again, MVAR suffers from the wider support of the wavelet, 3τ instead of 2τ. AVAR has a distinguished history of being the favorite tool of time keepers.

C. Detection of Slow Phenomena [Fig. 10(d)–(f)]

It is often useful to detect the corner where random walk or drift exceed the flicker floor, or where the drift exceeds
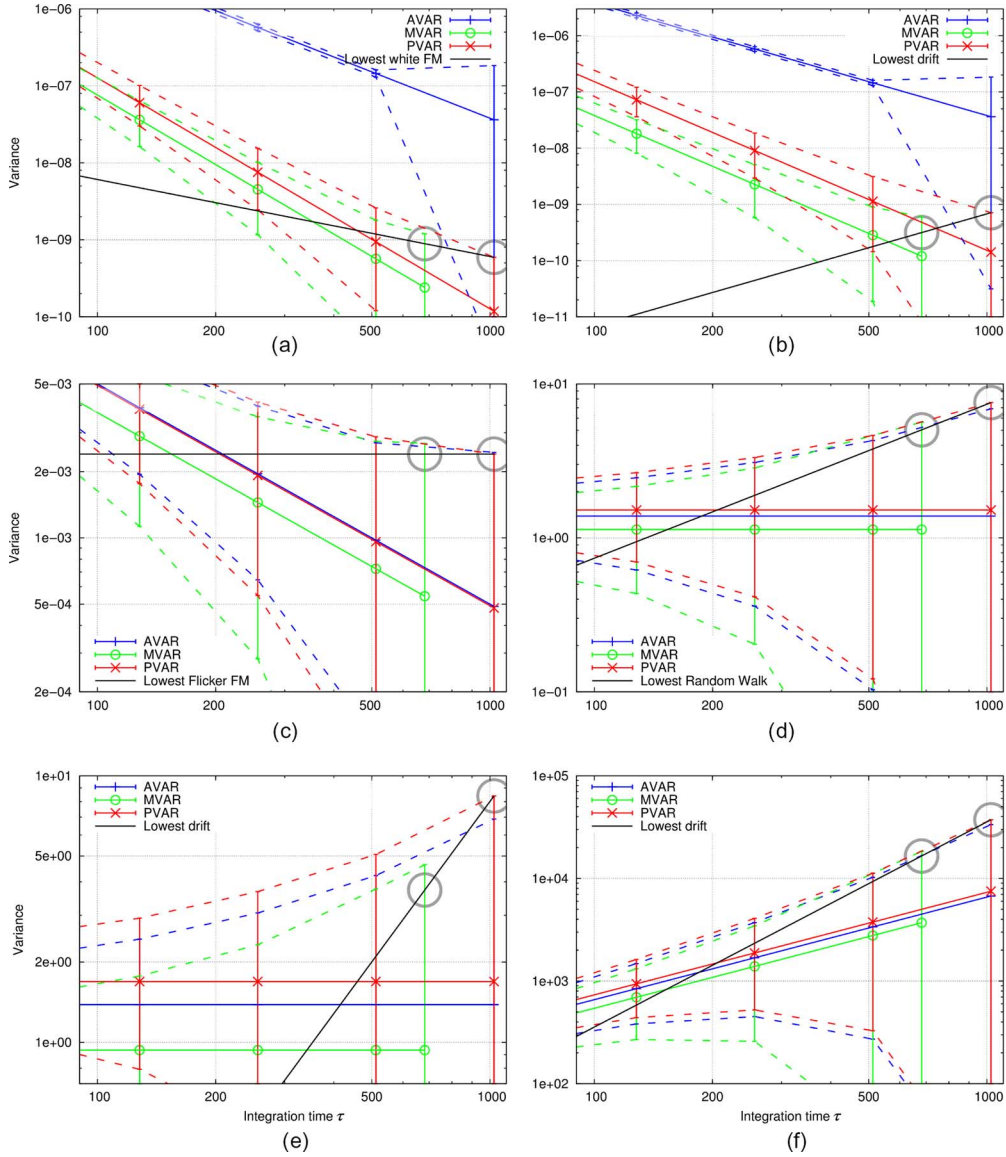
Fig. 10. Corner detection for the most common noise types (gray circles). The 97.5% upper bounds of the confidence intervals over the variance estimates are figured by dashed lines (blue for AVAR, green for MVAR, and red for PVAR). The lowest detected noise or drift by PVAR is represented as a solid black line. (a) White FM in white PM. (b) Drift in white PM. (c) Flicker FM in white FM. (d) Random walk in flicker FM. (e) Drift in flicker FM. (f) Drift in random walk.

the random walk. This problem is typical of Rb clocks and H masers, and also of precision oscillators based on mechanical properties of a resonator. Our simulation shows that AVAR is superior, but PVAR has a detection capability close to AVAR. Conversely, MVAR is the poorest choice.

VII. DISCUSSION AND CONCLUSION

PVAR is wavelet-like variance broadly similar to AVAR and MVAR, and intended for similar purposes. It derives from AVAR and MVAR after replacing the Π and Λ counter with the Ω counter, in turn based on the LR on phase data [9].

On closer examination, we notice that AVAR and MVAR address different problems. In the presence of white PM noise, MVAR has a dependence as $1/\tau^3$ instead of $1/\tau^2$. This is a good choice in microwave photonics and in other applications where the measurement of short-term stability is important. The

problem with MVAR is that the wavelet spans over 3τ instead of 2τ. Hence, AVAR is preferred for the measurement of long-term stability and in timekeeping, where the largest value of τ on the plot is severely limited by the length of the available data record. PVAR on the other hand is a candidate replacement for both because it features the $1/\tau^3$ dependence of MVAR and the 2τ measurement time of AVAR.

PVAR compares favorably to MVAR because it provides larger EDF, and in turn a smaller confidence interval. The objection that PVAR gives a larger response to the same noise level (right-hand column of Table I) is irrelevant because the response is just a matter of normalization. It is only in the region of fast processes that AVAR has higher EDF than PVAR (Fig. 8), but this happens where AVAR is certainly not the preferred option.

The best of PVAR is its power to detect and identify weak noise processes with the shortest data record. We have seen in

Section VI that PVAR is superior to MVAR in all cases, and also superior to AVAR for all short-term and medium-term processes, up to flicker FM included. AVAR is just a little better with random walk and drift.

In conclusion, theory and simulation suggest that PVAR is an improved replacement for MVAR in all cases, provided the computing overhead can be accepted. Whether or not AVAR is preferable to PVAR for timekeeping is a matter of discussion. AVAR renders the largest τ with a given data record. This is the case of random walk and drift. By contrast, PVAR is superior at detecting the frequency flicker floor, which is the critical parameter of the primary frequency standards used in timekeeping. These standards are supposed to be free from random walk and drift. Otherwise, when rendering the largest τ is less critical, PVAR is until now the best option.

ACKNOWLEDGMENTS

REFERENCES

[1] D. W. Allan, "Statistics of atomic frequency standards," *Proc. IEEE*, vol. 54, no. 2, pp. 222–231, Feb. 1966.

[2] J. J. Snyder, "Algorithm for fast digital analysis of interference fringes," *Appl. Opt.*, vol. 19, no. 4, pp. 1223–1225, Apr. 1980.

[3] D. W. Allan and J. A. Barnes, "A modified "Allan variance" with increased oscillator characterization ability," in *Proc. 35th Annu. Freq. Control Symp. (IFCS)*, Ft. Monmouth, NJ, USA, May 1981, pp. 470–474.

[4] J. J. Snyder, "An ultra-high resolution frequency meter," in *Proc. 35th Annu. Freq. Control Symp.*, May 27–29, 1981, pp. 464–489.

[5] D. B. Percival and A. T. Walden, *Wavelet Methods for Time Series Analysis*. Cambridge, U.K.: Cambridge Univ. Press, 2000.

[6] A. Papoulis, *The Fourier Integral and its Applications*. New York, NY, USA: McGraw Hill, 1962.

[7] J. G. Proakis and M. Salehi, *Communication System Engineering*, 2nd ed. Englewood Cliffs, NJ, USA: Prentice-Hall, 1994.

[8] G. Kramer and K. Klitsche, "Multi-channel synchronous digital phase recorder," in *Proc. IEEE Int. Freq. Control Symp.*, Seattle, WA, USA, Jun. 2001, pp. 144–151.

[9] E. Rubiola, M. Lenczner, P.-Y. Bourgeois, and F. Vernotte, "The omega counter, a frequency counter based on the linear regression," arXiv:1506.05009, Jun. 16 2015, *IEEE Trans. Ultrason., Ferroelectr., Freq. Control, Special Issue on the 2015 IFCS*, submitted for publication.

[10] E. Rubiola, "On the measurement of frequency and of its sample variance with high-resolution counters," *Rev. Sci. Instrum.*, vol. 76, no. 5, pp. 054703-1–054703-6, May 2005.

[11] S. T. Dawkins, J. J. McFerran, and A. N. Luiten, "Considerations on the measurement of the stability of oscillators with frequency counter," *IEEE Trans. Ultrason., Ferroelectr., Freq. Control*, vol. 54, no. 5, pp. 918–925, May 2007.

[12] E. Benkler, C. Lisdat, and U. Sterr. (2015, Apr.). *On the Relation Between Uncertainties of Weighted Frequency Averages and the Various Types of Allan Deviations* [Online]. Available: http://arxiv.org/pdf/1504.00466v3.pdf

[13] E. Benkler, E. Rubiola, U. Sterr, and F. Vernotte, private communication, International Frequency Control Symposium, Denver, CO, USA, Apr. 16, 2015.

[14] J. R. c. Vig, *IEEE Standard Definitions of Physical Quantities for Fundamental Frequency and Time Metrology—Random Instabilities, IEEE Standard* 1139–2008, Feb. 2009.

[15] J. A. Barnes *et al.*, "Characterization of frequency stability," *IEEE Trans. Instrum. Meas.*, vol. IM-20, no. 2, pp. 105–120, May 1971.

[16] J. Vanier and C. Audoin, *The Quantum Physics of Atomic Frequency Standards*. New York, NY, USA: Adam Hilger, 1989.

[17] P. Lesage and C. Audoin, "Characterization of frequency stability: Uncertainty due to the finite number of measurements," *IEEE Trans. Instrum. Meas.*, vol. 22, no. 2, pp. 157–161, Jun. 1973.

[18] O. E. Brigham, *The Fast Fourier Transform and its Applications*. Englewood Cliffs, NJ, USA: Prentice-Hall, 1988.

[19] L. Isserlis, "On certain probable errors and correlation coefficients of multiple frequency distributions with skew regression," *Biometrika*, vol. 11, no. 3, pp. 185–190, May 1916.

[20] L. Isserlis, "On a formula for the product-moment coefficient of any order of a normal frequency distribution in any number of variables," *Biometrika*, vol. 12, no. 1/2, pp. 134–139, Nov. 1918.

[21] C. Greenhall. (2015, Mar.). *'Greenhall's proof' in wikipedia entry 'Isserlis' theorem* [Online]. Available: http://en.wikipedia.org/wiki/Isserlis%27_theorem

[22] F. Vernotte, J. Delporte, M. Brunet, and T. Tournier, "Uncertainties of drift coefficients and extrapolation errors: Application to clock error prediction," *Metrologia*, vol. 38, no. 4, pp. 325–342, Dec. 2001.

[23] F. Vernotte and E. Lantz, "Metrology and 1/f noise: Linear regressions and confidence intervals in flicker noise context," *Metrologia*, vol. 52, no. 2, pp. 222–237, 2015.

[24] F. Vernotte, P. Y. Bourgeois, and F. Meyer. (2011). *SigmaTheta Software Package, GNU GPL/CeCILL License* [Online]. Available: theta.obs-besancon.fr/spip.php?article103

François Vernotte received the Ph.D. degree in engineering sciences from the University of Franche-Comté, Besançon, France, in 1991.

Since 1989, he has been with the Time and Frequency Team, Observatory of Besançon (now Observatory THETA/UTINAM), University of Franche-Comté. His research interests include long-term stability of oscillators such as atomic clocks and millisecond pulsars. His favorite tools are statistical data processing (time series, spectral analysis), parameter estimation (inverse problem, Bayesian statistics) and simulation (Monte-Carlo).

Michel Lenczner received the M.S. and Ph.D. degrees in numerical analysis from the University of Paris 6, Paris, France, in 1987 and 1991, respectively.

After receiving the Ph.D. degree, he became an Associate Professor in Applied Mathematics with the University of Franche-Comté, Besançon, France. He is currently a Professor of Mechanical Engineering with the Technical University of Belfort-Monbéliard, and a Researcher with the Micro-Acoustics Team, FEMTO-ST Laboratory, Besançon. His research interests include multiscale modeling and control of distributed mechatronic systems with an emphasis on micro- and nanosystems.

Pierre-Yves Bourgeois was born in Besançon, France, on February 29, 1976. He received the Ph.D. degree in 2004 from the University of Franche-Comté, Besançon, while he was studying ultrastable microwave cryogenic sapphire resonator oscillators at the LPMO (Laboratoire de Physique et de Métrologie des Oscillateurs).

After postdoctoral appointments in the Frequency Standards and Metrology Research Group of the University of Western Australia, he joined the Time and Frequency Department, CNRS, FEMTO-ST Institute, Besançon, France. He is currently investigating the definition of digital methods applied to modern techniques of time and frequency metrology and to the development of high precision instruments. He is also interested in atomic oscillators and ion trapped atomic clocks.

Dr. Bourgeois received IEEE's UFFC Best Student Award in 2004 for the development of ultra-low drift cryogenic sapphire resonator oscillators.

Enrico Rubiola received the M.S. degree in electronic engineering from the Politecnico di Torino, Torino, Italy, in 1983, the Ph.D. degree in metrology from Italian Ministry of Scientific Research, Rome, Italy, in 1989, and the Sc.D. degree in time and frequency metrology from the Université de Franche-Comté (UFC), Besançon, France, in 1999.

He has been a Researcher with the Politecnico di Torino, a Professor with the University of Parma, Parma, Italy, a Professor with the Université Henri Poincaré, Nancy, France, and a Guest Scientist with NASA Jet Propulsion Laboratory, Pasadena, CA, USA. Since 2005, he has been a Professor with the UFC and a Scientist with the FEMTO-ST Institute, Besançon, France, where he serves as Deputy Director of the Time and Frequency Department. He has investigated various topics of electronics and metrology, namely, navigation systems, time and frequency comparisons, atomic frequency standards, and gravity. His main fields of interest are precision electronics, phase-noise, amplitude-noise, frequency stability and synthesis, and low-noise oscillators from the low RF region to optics. He is the PI of the Oscillator IMP project, a platform for the measurement of short-term frequency stability and spectral purity.